






Molecular architecture of LSM14 interactions involved in the assembly of mRNA silencing complexes

Tobias Brandmann^{1,†}, Hana Fakim^{2,3,†} , Zoya Padamsi^{2,3}, Ji-Young Youn^{4,5}, Anne-Claude Gingras^{4,5}, Marc R Fabian^{2,3,*}  & Martin Jinek^{1,**} 

Abstract

The LSM domain-containing protein LSM14/Rap55 plays a role in mRNA decapping, translational repression, and RNA granule (P-body) assembly. How LSM14 interacts with the mRNA silencing machinery, including the eIF4E-binding protein 4E-T and the DEAD-box helicase DDX6, is poorly understood. Here we report the crystal structure of the LSM domain of LSM14 bound to a highly conserved C-terminal fragment of 4E-T. The 4E-T C-terminus forms a bi-partite motif that wraps around the N-terminal LSM domain of LSM14. We also determined the crystal structure of LSM14 bound to the C-terminal RecA-like domain of DDX6. LSM14 binds DDX6 via a unique non-contiguous motif with distinct directionality as compared to other DDX6-interacting proteins. Together with mutational and proteomic studies, the LSM14-DDX6 structure reveals that LSM14 has adopted a divergent mode of binding DDX6 in order to support the formation of mRNA silencing complexes and P-body assembly.

Keywords mRNA decapping; P-bodies; protein–protein interaction networks; SLiMs; translational repression

Subject Categories RNA Biology; Structural Biology

DOI 10.15252/emboj.201797869 | Received 27 July 2017 | Revised 19 January 2018 | Accepted 21 January 2018 | Published online 6 March 2018

The EMBO Journal (2018) 37: e97869

Introduction

Translational repression and mRNA turnover are central processes in post-transcriptional regulation of eukaryotic gene expression. Shortening of the 3' poly(A) tail of eukaryotic mRNAs is the initial and rate-limiting step of mRNA turnover and is carried out by the CCR4-NOT deadenylase complex (Chen &

Shyu, 2011). The deadenylated 3'-terminus subsequently serves as a binding platform for numerous protein factors promoting translational repression of the mRNA and facilitating the irreversible removal of the 5'-terminal cap structure by the Dcp1–Dcp2 decapping complex. Ultimately, decapped mRNAs are degraded by the 5'–3' exonuclease XRN1 and removed from the translational pool (Chowdhury & Tharun, 2009). The recruitment of the decapping complex to the 5'-terminal cap structure is orchestrated by an intricate, dynamic network of protein–protein interactions involving various decapping factors and translational repressors. These include the LSM1-7 complex, PATL1, enhancer of decapping 3 (EDC3), EDC4, the eIF4E-binding protein 4E-T, Like Sm14 (LSM14), and the DEAD-box RNA helicase DDX6 (Arribas-Layton *et al*, 2013; Nishimura *et al*, 2015). Most of the translational repressors and decapping activators have a modular architecture in which conserved globular protein domains are embedded within low-complexity sequence stretches that are predicted to be unstructured (Jonas & Izaurralde, 2013). Intriguingly however, these intrinsically disordered protein regions often contain highly conserved short linear sequence motifs (SLiMs) that mediate protein complex assembly, as well as the formation of ribonucleoprotein (RNP) granules such as processing bodies (P-bodies; Eulalio *et al*, 2007a).

One of the key components in the assembly of the mammalian gene silencing complexes is LSM14 (also known as RAP55), a member of the like-Sm (LSM) protein family that is highly conserved from yeast to humans (Marnef *et al*, 2009). The N-terminal LSM domain of LSM14 is a common fold among decapping factors and is also found in the LSM1-7 proteins and EDC3. However, in contrast to LSM1-7 proteins, whose LSM domains interact to form a heteroheptameric ring-like structure with RNA-binding properties, the LSM domains in LSM14 and EDC3 diverge functionally and serve as interaction platforms for other protein factors (Tritschler *et al*, 2007, 2008). In addition to its N-terminal LSM

1 Department of Biochemistry, University of Zurich, Zurich, Switzerland

2 Department of Oncology, McGill University, Montreal, QC, Canada

3 Segal Cancer Centre, Lady Davis Institute for Medical Research, Jewish General Hospital, Montreal, QC, Canada

4 Lunenfeld-Tanenbaum Research Institute, Mount Sinai Hospital, Toronto, ON, Canada

5 Department of Molecular Genetics, University of Toronto, Toronto, ON, Canada

*Corresponding author. Tel: +1 514 340 8222; E-mail: marc.fabian@mcgill.ca

**Corresponding author. Tel: +41 44 635 5572; E-mail: jinek@bioc.uzh.ch

†These authors contributed equally to this work

domain, LSM14 also contains a central phenylalanine–aspartate–phenylalanine (FDF) motif, which interacts with DDX6, and C-terminal RGG motifs that are methylated by the protein arginine methyltransferase 1 (PRMT1; Matsumoto *et al*, 2012). Additionally, two highly conserved sequence stretches downstream of the FDF motif, the FFD and TFG motifs, have been identified (Fig 1A; Albrecht & Lengauer, 2004). The roles of these latter motifs in LSM14 function, however, remain to be established.

The yeast LSM14 homolog SCD6 has been reported to enhance mRNA decapping *in vitro*. In addition, SCD6 and the *Xenopus* homolog, xRAP55a, have been reported to repress translation (Yang *et al*, 2006; Fromm *et al*, 2012; Rajyaguru *et al*, 2012), and SCD6 has been shown to bind eIF4G via its methylated RGG motifs (Rajyaguru *et al*, 2012). Whether this interaction is conserved in higher eukaryotes, however, is not known. Metazoan LSM14 orthologs interact with a number of multiple mRNA silencing factors, including 4E-T and DDX6, which are involved in translational repression and decay mRNAs targeted by the CCR4-NOT complex (Coller & Parker, 2005; Tritschler *et al*, 2009; Carroll *et al*, 2011; Matsumoto *et al*, 2012; Sweet *et al*, 2012; Nishimura *et al*, 2015). We recently reported that the LSM domain of LSM14 directly interacts with two independent regions of 4E-T (middle-motif: residues 335–490; C-terminal motif: residues 948–985) via its LSM domain (Nishimura *et al*, 2015). DDX6 serves as a protein interaction hub for several translational repressors and enhancers of mRNA decapping, such as LSM14, 4E-T, PATL1, and EDC3 (Tritschler *et al*, 2008, 2009; Sharif *et al*, 2013; Ozgur *et al*, 2015). LSM14 employs its FDF motif to interact with the C-terminal RecA domain of DDX6 (Tritschler *et al*, 2009). Notwithstanding these data, it is currently unclear as to exactly how LSM14 interfaces with both 4E-T and DDX6.

Here we set out to obtain structural and biochemical insights into how human LSM14 interfaces with the mRNA silencing machinery. To this end, we solved the crystal structures of LSM14 bound to 4E-T and to DDX6. Our study shows that the evolutionarily conserved C-terminus of 4E-T wraps around the LSM domain of LSM14. Furthermore, we show that LSM14 employs both its FDF and TFG motifs to bind the C-terminal RecA domain of DDX6 via a bipartite interaction. We show that both interactions are underpinned by extensive hydrophobic interactions between evolutionarily conserved sequence motifs and common structural domains. Finally, we reveal that the unique architecture of the LSM14–DDX6 interaction serves to present the highly conserved FFD motif of LSM14 as an additional recruitment platform for the decapping activator EDC4.

Results

Extensive hydrophobic interactions anchor 4E-T to the N-terminal LSM domain of LSM14

We recently showed that the N-terminal LSM domain of LSM14 directly interacts with two conserved sites in the eIF4E-binding protein 4E-T: a central region spanning residues 335–490 and a C-terminal region comprising residues 948–985 (Fig EV1A; Nishimura *et al*, 2015). To gain structural insights into these interactions, we determined the crystal structure of the minimal LSM14–4E-T

complex composed of the N-terminal LSM domain of human LSM14 (LSM14_{LSM}; residues 1–84) and a C-terminal 4E-T fragment (4E-T_C; residues 954–985; Fig 1A and B). The structure was solved at a resolution of 2.6 Å by single-wavelength anomalous diffraction (SAD) using a selenomethionine-substituted 4E-T_C construct in which an additional methionine residue (V963M) was introduced by site-directed mutagenesis (Table 1). The crystal structure reveals a tetrameric complex with 2:2 stoichiometry in which each LSM14 is simultaneously bound by two 4E-T protomers (Fig EV1B). To ascertain whether the observed quaternary structure occurs in solution, we made use of multi-angle light scattering (MALS) to determine the molecular weight of the LSM14_{LSM}–4E-T_C complex. MALS analysis indicated a combined molecular weight of 12.9 kDa (Fig EV1C) corresponding to a 1:1 complex, which suggests that the 2:2 tetramer is a result of crystallization-induced domain swapping. To reconstruct the likely solution structure of the LSM14_{LSM}–4E-T_C complex, we combined the fragments from the two 4E-T_C molecules (corresponding to residues 954–973 and 974–985) that contact each LSM14_{LSM} molecule in a single composite model (Fig 1C).

The N-terminal LSM domain of LSM14 adopts a typical LSM domain fold comprising an open five-stranded β-barrel-like structure similar to previously reported structures of the LSM domains of the human enhancer of decapping EDC3 and *Drosophila melanogaster* TraI, an LSM14 homolog (Figs 1C–E and EV1D; Tritschler *et al*, 2007; Fromm *et al*, 2012), superimposing with root-mean-square deviations (RMSDs) of 1.7 and 2.4 Å, respectively (over 72 and 88 Cα atoms). Canonical SM and LSM proteins such as SmD3 and LSM1-7 oligomerize via an antiparallel interaction of the β-strands β4 and β5 (Kambach *et al*, 1999; Tritschler *et al*, 2007; Jonas & Izaurralde, 2013). In contrast, both LSM14 and EDC3 are monomeric and lack an N-terminal α-helix, a hallmark of canonical LSM proteins that contributes to their assembly in ring-shaped oligomers (Figs 1C, and EV1D and E). These features enable LSM14 and EDC3 to function as standalone protein interaction platforms, instead of forming ring-like heptamers with RNA-binding interfaces.

The 4E-T_C fragment wraps around the LSM domain in an extensive interaction that involves more than 70% of its residues, burying ~1,300 Å² of solvent-accessible surface area. The N-terminal portion of 4E-T_C (residues 954–974) binds in a mostly extended conformation, while the C-terminal part (residues 975–985) forms a short beta strand followed by an α-helical motif. The LSM14_{LSM}–4E-T_C interaction is mediated mainly by the insertion of conserved hydrophobic residues from 4E-T_C into two hydrophobic cavities found at opposite ends of the LSM domain β-barrel (Figs 1C–E and 2A). The conserved residues Leu955^{4E-T}, Trp958^{4E-T}, and Phe959^{4E-T} in the extended N-terminal part of 4E-T_C occupy a cavity lined with Leu26^{LSM14}, Ile29^{LSM14}, Val36^{LSM14}, Ile72^{LSM14}, and Leu75^{LSM14}. This region is additionally anchored by van der Waals contacts between Met971^{4E-T} and Thr35^{LSM14}, Ala37^{LSM14} and Ile66^{LSM14} (Fig 2A). The C-terminal helical element of 4E-T_C is fixed on the LSM14_{LSM} surface by interactions of Val978^{4E-T} and Leu981^{4E-T} with a hydrophobic patch formed by Tyr22^{LSM14}, Phe62^{LSM14}, Ile65^{LSM14}, and Phe67^{LSM14} (Fig 2A). This interaction is further reinforced by hydrogen-bonding interactions between Glu982^{4E-T} and Ser16^{LSM14} and Tyr22^{LSM14}. The N- and C-terminal hydrophobic motifs in 4E-T_C are connected by a short β-strand (residues Ile976^{4E-T}–Val978^{4E-T}) that

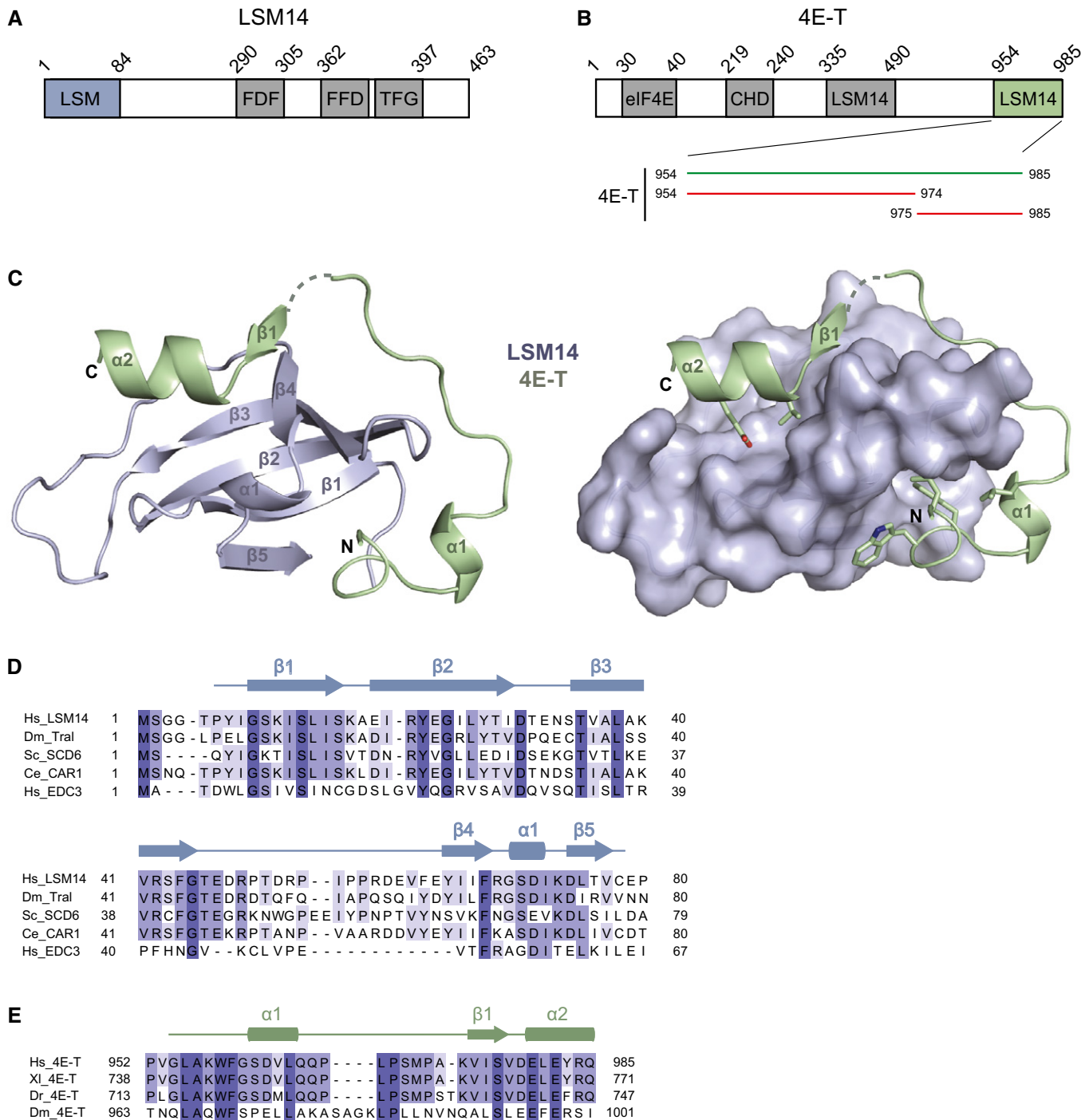


Figure 1. Structure of the N-terminal LSM domain of LSM14 in complex with a conserved C-terminal fragment of 4E-T.

- A Schematic diagram of LSM14. The N-terminal LSM domain and FDF, FFD, and TFG motifs are indicated (not to scale).
- B Schematic diagram of full-length 4E-T and 4E-T fragments used for MBP pull-down experiments in Fig 2B. Coordinates are indicated on the left and right of each fragment. The indicated regions (not to scale) are as follows: eIF4E, binding site for eIF4E; CHD, cup homology domain; LSM14, LSM14-interacting site.
- C Crystal structure of the N-terminal LSM domain of human LSM14 in complex with a conserved C-terminal 4E-T fragment. The diagram depicts the likely solution structure obtained by combining two fragments of 4E-T_C that undergo crystallization-induced domain swapping, as indicated by dashed line. Left: Cartoon representation of the complex. Right: LSM domain of LSM14 shown in surface representation and 4E-T_C residues critical for complex formation are shown as sticks. Secondary structure elements are labeled according to (D) and (E).
- D Sequence alignment of conserved amino acids within the LSM domains of human (Hs) LSM14, *Drosophila melanogaster* (Dm) Tral, yeast (Sc) SCD6, *Caenorhabditis elegans* (Ce) CAR1, and human (Hs) EDC3. Secondary structure elements with corresponding numbering are indicated above the sequence.
- E Sequence alignment of conserved amino acids within the C-terminal motifs of human (Hs), *Xenopus laevis* (Xl), zebrafish (Dr), and *D. melanogaster* (Dm) 4E-T proteins. Secondary structure elements with corresponding numbering are indicated above the sequence.

Table 1. Crystallographic data collection and refinement statistics.

Dataset	DDX6 _C -LSM14 _{FDF-TFG}	LSM14 _{LSM} -4E-T _C
	Native	SeMet SAD
X-ray source	SLS X06DA (PXIII)	SLS X06DA (PXIII)
Space group	<i>P6</i> ₂ 2	<i>P4</i> ₂ 2
Cell dimensions		
<i>a</i> , <i>b</i> , <i>c</i> (Å)	92.15, 92.15, 149.90	64.89, 64.89, 61.67
α , β , γ (°)	90, 90, 120	90, 90, 90
Wavelength (Å)	0.979340	0.979090
Resolution (Å) ^a	46.07–3.03 (3.14–3.03)	45.88–2.62 (2.72–2.62)
<i>R</i> _{merge} ^a	0.108 (1.118)	0.090 (0.657)
CC1/2 ^a	0.999 (0.875)	1.000 (0.982)
<i>I</i> / σ ^a	31.5 (3.5)	54.4 (8.6)
Observations ^a	147,658 (15,066)	212,500 (21,151)
Unique reflections ^a	7,824 (762)	4,287 (418)
Multiplicity ^a	18.9 (19.7)	49.6 (50.1)
Completeness (%) ^a	99.8 (99.4)	99.7 (99.1)
Refinement		
Resolution (Å)	46.07–3.03	45.88–2.62
No. reflections	7,824 (762)	4,279 (418)
<i>R</i> _{work} / <i>R</i> _{free}	0.204/0.242	0.221/0.245
No. atoms		
Protein	1,734	844
Ligands	10	
Water	1	
B-factors		
Mean	71.5	68.0
Protein	71.3	68.0
Ligands	102.8	
Water	46.5	
R.m.s. deviations		
Bond lengths (Å)	0.003	0.003
Bond angles (°)	0.48	0.77
Ramachandran plot		
% Favored	97.1	97.1
% Allowed	2.9	2.9
% Outliers	0.0	0.0

^aValues in parentheses denote highest resolution shell.

runs parallel to LSM14 strand β ₄, forming hydrogen-bonding interactions to the polypeptide backbone of residues Tyr64^{LSM14}–Ile66^{LSM14}. Additional interactions involving Met963^{4E-T} and Leu968^{4E-T} with Leu26^{LSM14} and Ile29^{LSM14} stabilize a sharp turn in 4E-T_C around the surface of LSM14_{LSM} that connects the two main interacting regions.

The structure of the LSM14_{LSM}-4E-T_C complex reveals that the interaction between LSM14 and 4E-T relies on multiple molecular contacts converging on the two hydrophobic interaction hotspots on the surface of the LSM domain of LSM14. This is supported by

the observation that both the N- and C-terminal portions of 4E-T_C are required for stable interaction between LSM14_{LSM} and 4E-T_C *in vitro* (Fig 2B). To further delineate the contributions of individual amino acid residues, we tested the binding of wild-type and mutant 4E-T proteins in a pull-down assay using recombinant maltose binding protein (MBP)-tagged LSM14_{LSM} and glutathione S-transferase (GST)-tagged 4E-T_C fragments (Fig 2C). Individual alanine substitutions of Trp958^{4E-T} or Phe959^{4E-T} in GST-4E-T_C were sufficient to abrogate the interaction with LSM14_{LSM}, as was the substitution of Glu982^{4E-T} with lysine. Additionally, tandem alanine substitutions of Trp958^{4E-T} and Leu955^{4E-T}, as well as Val978^{4E-T} and Leu981^{4E-T} also led to loss of LSM14_{LSM} binding. In contrast, alanine substitutions of serine residues Ser970^{4E-T} or Ser961^{4E-T}, which do not mediate specific contacts with LSM14_{LSM}, did not affect binding. We additionally quantified the binding affinity of LSM14_{LSM} for 4E-T_C by isothermal titration calorimetry (ITC). LSM14_{LSM} and 4E-T_C interacted with a *K*_d of 0.3 μ M, whereas a 4E-T_C mutant containing an alanine substitution of Trp958^{4E-T} was unable to bind to LSM14_{LSM} (Table 2 and Fig EV1F). Together, these results indicate that 4E-T_C residues making specific contacts with either of the two hydrophobic surfaces in the LSM14 LSM domain are required for the interaction. Corroborating this result, alanine substitutions of either Tyr22^{LSM14} or Ile29^{LSM14} in the two hydrophobic pockets in LSM14_{LSM} that interact with 4E-T_C were sufficient to abrogate interactions with 4E-T_C *in vitro* (Fig 2D).

We also disrupted the hydrophobic pockets in the LSM14_{LSM} domain in the context of full-length LSM14 to determine whether this affects the 4E-T interaction *in vivo*. To this end, HeLa cell lines were generated that stably express FLAG-tagged wild-type LSM14 or the Y22E/I29E mutant. FLAG-LSM14 proteins were immunoprecipitated from benzonase-treated cell lysates with anti-FLAG antibody, and LSM14-interacting proteins were resolved by SDS-PAGE and analyzed by Western blotting (Fig 2E). Wild-type LSM14 co-precipitated both 4E-T and DDX6. In contrast, the Y22E/I29E LSM14 mutant failed to interact with endogenous 4E-T, even though DDX6 binding was not perturbed, indicating that the hydrophobic interaction hotspots in the LSM domain of LSM14 are required for the interaction with 4E-T *in vivo*. Together with our previous observations that the LSM domain of LSM14 interacts with both the middle and C-terminal regions of 4E-T, these results suggest that both LSM14-interaction motifs in 4E-T function redundantly and bind to LSM14 in a similar manner.

A previous study demonstrated that *Xenopus* (x)LSM14 represses bound transcripts in oocytes, and that this repression was mediated by an N-terminal region in xLSM14 (Tanaka *et al*, 2006). As our data demonstrate that the N-terminal LSM domain directly binds to 4E-T, we tested whether this interaction plays a role in mRNA repression. To this end, we used the bacteriophage λ N-BoxB tethering system in HeLa cells to tether the LSM14 LSM domain to a Renilla luciferase (RL) reporter mRNA. Tethering λ NHA-tagged LSM14_{LSM} (WT) to the RL-5BoxB reporter mRNA repressed RL expression ~threefold when compared to tethering LacZ (Figs 2F and EV1G). In contrast, the Y22E/I29E LSM domain mutant that cannot interact with 4E-T did not efficiently silence reporter mRNA translation. These results thus demonstrate that the LSM14-4E-T interaction plays a role in repressing mRNAs associated with LSM14.

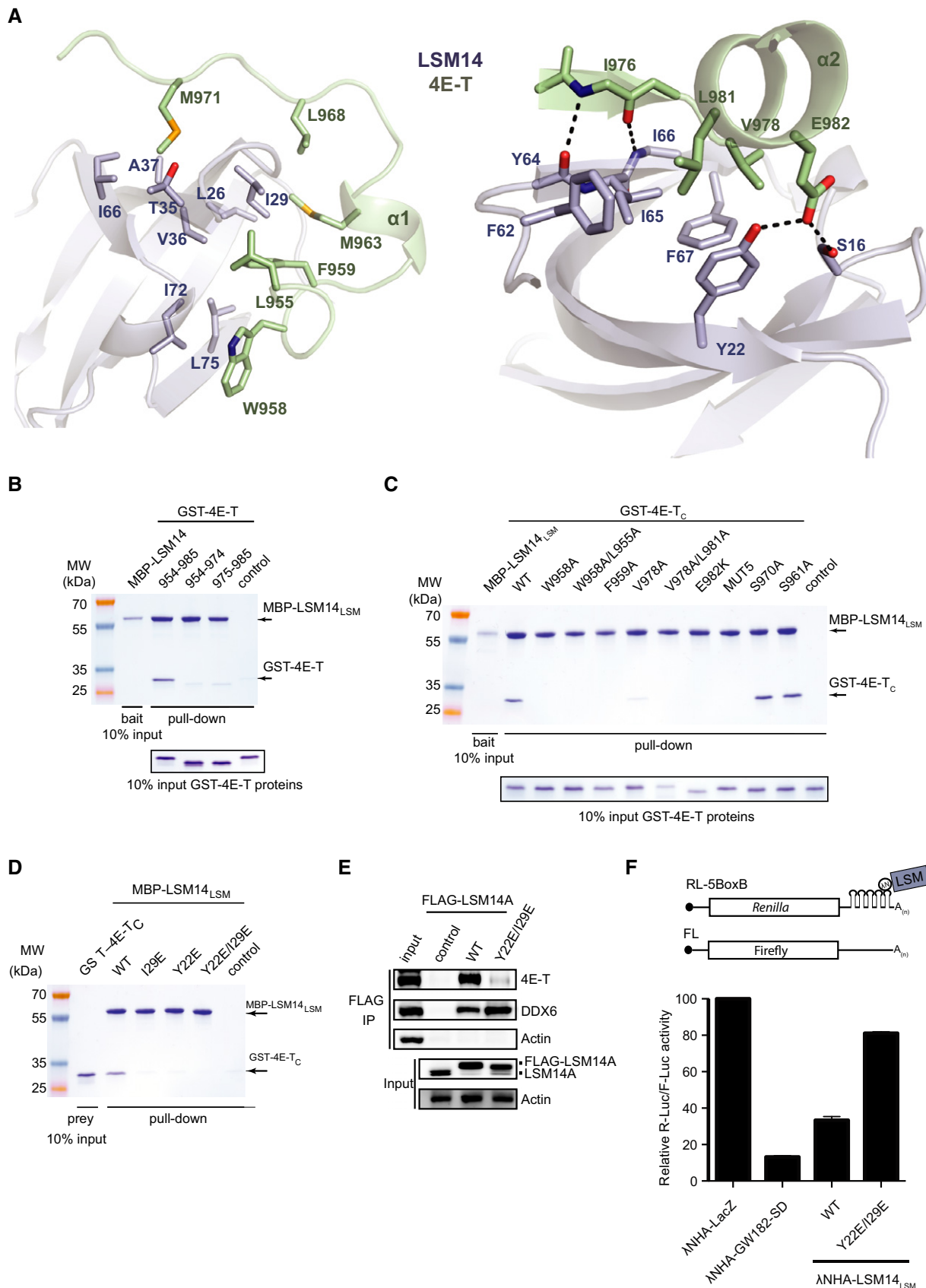


Figure 2.

Figure 2. LSM14–4E-T complex formation is mediated by extensive hydrophobic interactions.

- A Close-up views of the interface between the LSM14 domain (light blue) and 4E-T peptide (green). Interacting side chains of LSM14 and 4E-T are shown as sticks and labeled by single letter code. Dashed lines indicate hydrogen-bonding interactions, and secondary structures elements are numbered as in Fig 1D and E.
- B SDS–PAGE analysis of input (lower image) and MBP pull-down experiments (upper image) using recombinant MBP-LSM14 protein (MBP-LSM14_{LSM}, residues 1–84) immobilized on amylose-beads and incubated with recombinant GST-tagged C-terminal 4E-T fragments. MW, molecular weight markers.
- C SDS–PAGE analysis of input (lower image) and pull-down experiments (upper image) using recombinant MBP-LSM14 protein (MBP-LSM14_{LSM}, residues 1–84) immobilized on amylose-beads and incubated with recombinant wild-type or mutant GST-tagged C-terminal 4E-T (4E-T_C, residues 954–985) protein constructs. MUTS, 4E-T_C L955A/W958A/F959A/V978A/L981A.
- D SDS–PAGE analysis of pull-down experiments using recombinant wild-type or mutant MBP-LSM14_{LSM} constructs immobilized on amylose-beads and incubated with recombinant wild-type GST-tagged 4E-T_C fragment. MBP-LSM14_{LSM} variants are indicated above the gel.
- E Immunoprecipitation (IP) of wild-type and mutant FLAG-LSM14A proteins from benzonase-treated HeLa cell extracts using anti-FLAG antibody. Immunoprecipitated complexes were separated by SDS–PAGE and probed with antibodies against the indicated proteins.
- F Luciferase reporter assays using HeLa cells co-transfected with plasmids coding for RL-5BoxB and FL reporters and plasmids expressing λNHA fusions of the wild-type (WT) LSM14_{LSM} domain or a Y22E/I29E mutant. A plasmid expressing the silencing domain of GW182 was used as a positive control (Zipprich *et al*, 2009; Fabian *et al*, 2011). λNHA-LacZ served as a negative control. Activity of RL was normalized to expression of FL. Values represent relative RL activities normalized to FL with expression in the presence of λNHA-LacZ set as 100%. Values represent means (±SEM) from triplicate experiments.

Source data are available online for this figure.

Table 2. Equilibrium dissociation constants for LSM14 and DDX6 interactions.

Interaction	K_d (μM)
LSM14 _{LSM} –4E-T _C	0.30 ± 0.06
DDX6 _C –LSM14 _{FDF-TFG}	1.62 ± 0.15
DDX6 _C –PATL1 _{TFG-FDF}	0.23 ± 0.04
DDX6 _C –PATL1 _{TFG} LSM14 _{FDF}	0.04 ± 0.01
DDX6 _C –EDC3 _{TFG-FDF}	0.41 ± 0.04
DDX6 _C –4E-T _{WFS-IEL}	0.39 ± 0.10

LSM14 uses conserved non-contiguous FDF and TFG motifs to bind DDX6

The C-terminal RecA-like domain of the RNA DEAD-box helicase DDX6 (DDX6_C) serves as a binding platform for the CNOT1 subunit of the CCR4-NOT complex, as well as for a number of translational repressors and mRNA decapping factors including PATL1, EDC3, 4E-T, and LSM14 (Fig 3A; Tritschler *et al*, 2009). The FDF motif of the *D. melanogaster* LSM14 homolog Tral has previously been shown to be required in order for Tral to interact with DDX6_C (Tritschler *et al*, 2009). Two other highly conserved short motifs are found downstream of the FDF, namely the FFD and TFG motifs (Figs 3B and 4A; Albrecht & Lengauer, 2004; Marnef *et al*, 2009). However, the functions of these LSM14 motifs are not known. We utilized conventional affinity purification followed by immunoblotting to determine whether deleting these conserved sequences impairs LSM14 interactions with known interacting proteins such as 4E-T, PATL1, and DDX6. To this end, HeLa cell lines were generated in which endogenous LSM14 was stably depleted by RNA interference and complemented with FLAG-tagged wild-type (WT) LSM14 or a LSM14 mutant lacking both the FFD and TFG motifs (LSM14_{ΔFFD-TFG}). Affinity purification of wild-type FLAG-LSM14 resulted in co-precipitation of 4E-T, PATL1, and DDX6 (Fig 3C). In stark contrast, a LSM14 mutant lacking both the FFD and TFG motifs (LSM14_{ΔFFD-TFG}) failed to co-precipitate DDX6, yet associated with PATL1 and 4E-T as efficiently as wild-type LSM14. Deleting just the FFD motif from LSM14 (LSM14_{ΔFFD}) did not interfere with DDX6 association, whereas a LSM14 mutant lacking the

TFG motif alone (LSM14_{ΔTFG}) failed to interact with DDX6 (Fig 3C).

To determine whether LSM14 utilizes its TFG motif to directly bind DDX6, we performed *in vitro* pull-down experiments using recombinant C-terminal RecA domain of DDX6 (DDX6_C) fused to an N-terminal MBP tag and a series of glutathione S-transferase (GST)-fused LSM14 fragments. GST-LSM14 protein containing the FDF, FFD, and TFG motifs efficiently bound MBP-DDX6_C, while LSM14 fragments lacking either the FDF or TFG motifs did not (Fig 3D). Additionally, an LSM14 construct lacking the region interspersing the FDF and the FFD motifs (Δ324–358) bound MBP-DDX6_C as efficiently as the wild-type GST-LSM14 construct. Taken together, these results show that LSM14 requires both its FDF and TFG motifs for stable interaction with DDX6_C, while the conserved FFD motif is dispensable for the interaction.

Structure of a LSM14 peptide in complex with the DDX6 C-terminal RecA domain

Unlike EDC3, whose FDF motif is sufficient for a stable interaction with DDX6 (Tritschler *et al*, 2008, 2009), LSM14 requires both its FDF and TFG motifs to bind DDX6. To gain insight into the LSM14–DDX6 interaction, we sought to determine the crystal structure of the C-terminal RecA domain of human DDX6 (DDX6_C, residues 303–469) bound to a fragment of LSM14 encompassing the FDF, FFD, and TFG motifs. The FDF and FFD motifs in the human LSM14 protein are connected by a long linker region, which is predicted to be unstructured (Fig 4A). To facilitate crystallization, we instead used the *Caenorhabditis elegans* LSM14 ortholog Car-1, which contains a much shorter linker (Fig 4A). The structure of the DDX6_C–Car-1_{FDF-TFG} complex was determined at a resolution of 3.0 Å (Fig 4B and C, Table 1). The FDF, FFD, and TFG motifs of Car-1 and human LSM14 are highly conserved in sequence, implying that the binding of human LSM14 can be readily extrapolated from the structure based on sequence alignment (Fig 4A). Henceforth, we use the sequence numbering of the human LSM14 protein when describing the structure for the sake of clarity.

In the complex, DDX6_C adopts a typical RecA-like fold, composed of a central flat beta-sheet composed of six parallel beta-strands, which are sandwiched between two helical layers, composed of five alpha-helices, as described previously. The

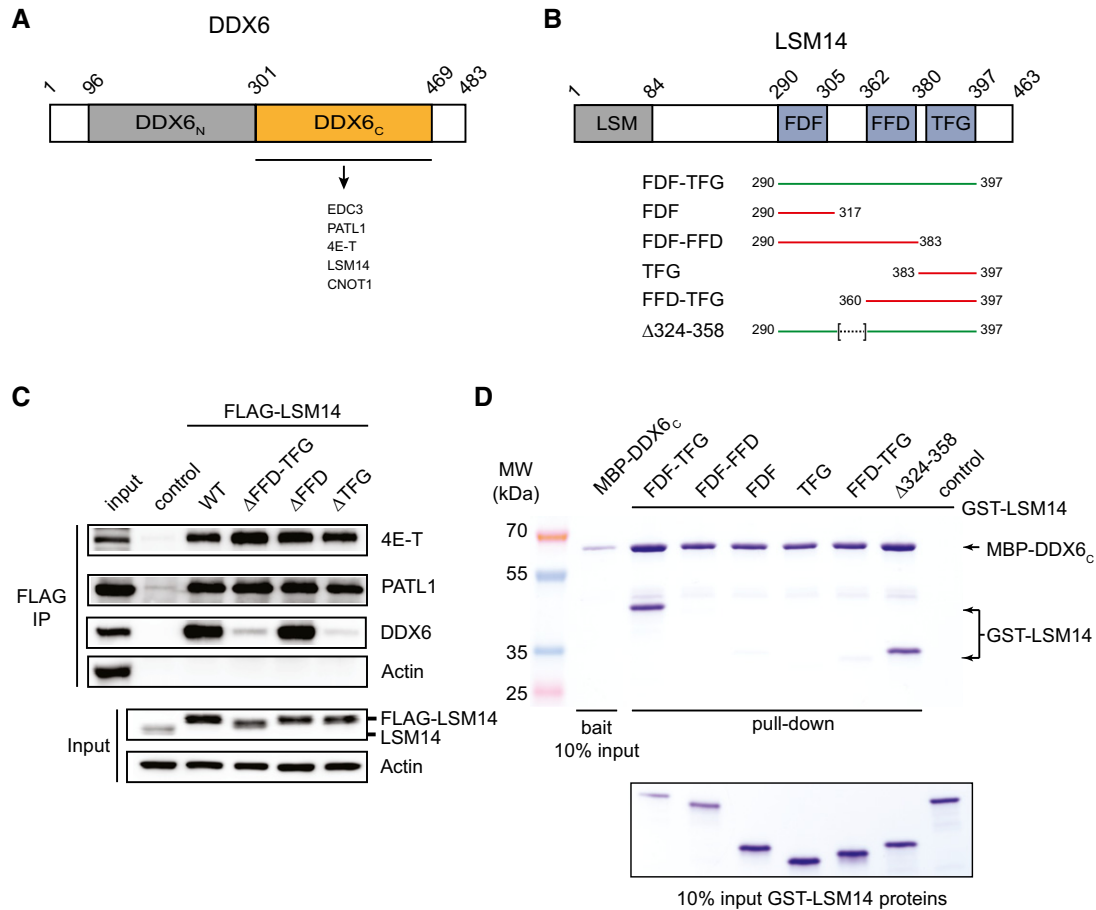


Figure 3. The LSM14 FDF and TFG motifs interact with the C-terminal RecA-like domain of DDX6.

- A Schematic diagram of the domain organization in human DDX6. N- and C-terminal RecA (DDX6_N and DDX6_C) domains are labeled as such. Proteins that interact with DDX6_C are denoted.
- B Schematic diagram of the domain organization of human LSM14. LSM14 constructs used for immunoprecipitations and pull-down experiments in (C, D) are indicated.
- C Immunoprecipitation (IP) of wild-type and mutant FLAG-LSM14A proteins from benzonase-treated HeLa cell extracts using anti-FLAG antibody. Immunoprecipitated complexes were separated by SDS-PAGE and probed with antibodies against indicated proteins.
- D SDS-PAGE analysis of input (lower) and pull-down experiments (upper) using recombinant wild-type MBP-DDX6_C immobilized on amylose-beads and incubated with indicated GST-tagged LSM14 fragments as described in (B).

Source data are available online for this figure.

DDX6_C-LSM14_{FDF-TFG} interaction interface buries 1,200 Å² of solvent-exposed surface area. The structure of the complex reveals a bipartite binding mode mediated by two discontinuous segments in LSM14 that engage in extensive interactions with DDX6_C (Fig 4C). The N-terminal segment, which contains the FDF motif and includes residues 290–313, adopts an extended conformation, followed by an alpha-helical element. The C-terminal segment containing the TFG motif forms an alpha-helix and corresponds to residues 384–397. The two segments are interspaced by an unstructured region corresponding to residues 314–383 in human LSM14 that harbors the FFD motif.

The interaction between DDX6_C and LSM14_{FDF-TFG} is driven mainly by extensive hydrophobic interactions mediated by evolutionarily conserved residues in the FDF and TFG motifs. Similar to previously reported crystal structures of DDX6_C bound to 4E-T and

EDC3 (Tritschler *et al*, 2009; Ozgur *et al*, 2015), LSM14_{FDF-TFG} uses its FDF motif to interact with a hydrophobic pocket on the surface of DDX6_C. Here, Phe296^{LSM14} and Phe298^{LSM14} of the FDF are contacted by the conserved residues Ala314^{DDX6}, Val316^{DDX6}, Cys324^{DDX6}, Leu328^{DDX6}, Ile460^{DDX6} (Fig 4C). The helical element downstream of the FDF motif is anchored via its highly conserved Phe305^{LSM14} by hydrophobic interactions with a second pocket lined with Tyr315^{DDX6}, Ile438^{DDX6}, and Leu446^{DDX6} (Fig 4C).

The TFG motif in the C-terminal segment of LSM14_{FDF-TFG} forms an alpha-helix upon binding to DDX6_C (Fig 4C). This helical element interacts with an additional hydrophobic pocket comprised of Glu318^{DDX6}, Arg319^{DDX6}, Val322^{DDX6}, Arg346^{DDX6}, Leu349^{DDX6}, Leu350^{DDX6}, and Lys353^{DDX6}, which anchors Phe396^{LSM14} of the TFG motif. Thr395^{LSM14} is at the center of a hydrogen bond network with Arg346^{DDX6} and Glu318^{DDX6}. Together, the extensive interactions

centered on the conserved TFG motif underscore its importance for the LSM14–DDX6_C interaction. The interactions mediated by the TFG motif are additionally supported by hydrogen-bonding interactions of Asn392^{LSM14} with Arg346^{DDX6} and Gln345^{DDX6}, respectively, and a salt bridge formed by Glu394^{LSM14} and Arg319^{DDX6}.

To corroborate our structural observations, we generated mutant human LSM14 proteins harboring specific point mutations in key interacting residues and tested their binding to DDX6 in pull-down assays *in vitro* and in cell lysates (Fig 5A and B). In keeping with previous reports (Tritschler *et al*, 2009), alanine substitutions of

Phe296^{LSM14} and Phe298^{LSM14} in the FDF motif resulted in the loss of interaction with DDX6 both *in vitro* and *in vivo* (Fig 5A and B). Alanine substitution of Phe305^{LSM14} also disrupted DDX6_C binding *in vitro*. Mutating the TFG motif by alanine substitutions of Glu394^{LSM14}, Thr395^{LSM14}, Phe396^{LSM14}, and Gly397^{LSM14} (ETFG to AAAA) also abolished interactions with DDX6 in cells (Fig 5B), confirming the requirement of the TFG motif for the LSM14–DDX6 interaction. Indeed, alanine substitution of Phe396^{LSM14} alone was sufficient to disrupt DDX6 binding *in vitro* and in cells (Fig 5A and B). In line with a previous finding, the LSM14 FFD motif was

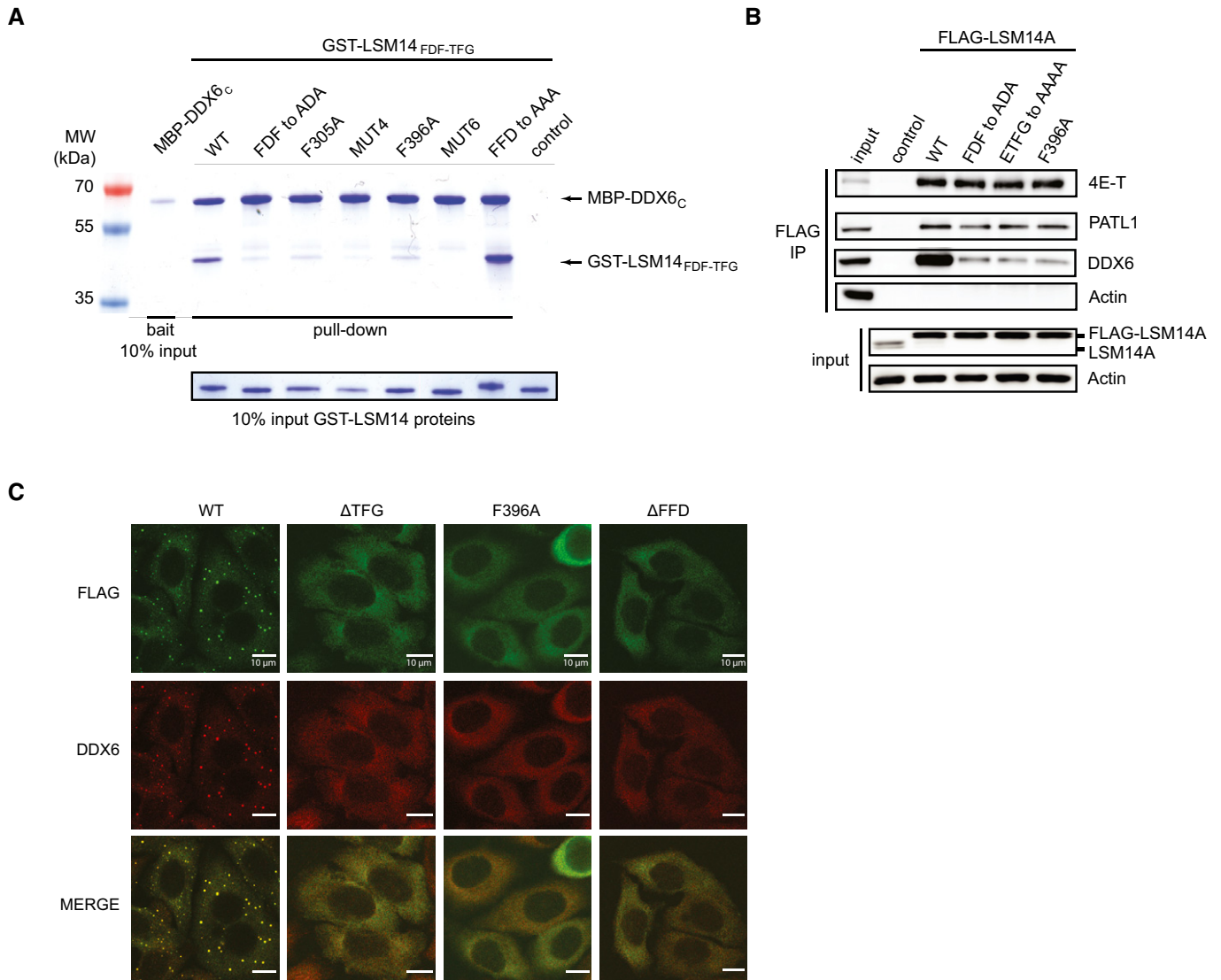


Figure 5. The DDX6–LSM14 interaction is necessary for P-body assembly.

A SDS–PAGE analysis of input (lower image) and pull-down experiment (upper image) using recombinant MBP-DDX6_C protein immobilized on amylose-beads and incubated with recombinant GST-LSM14_{FDF-TFG} (residues 290–397) protein constructs. Substitutions in GST-LSM14_{FDF-TFG} variants are indicated. MUT4, F292A/F296A/F298A/F305A; MUT6, F292A/F296A/F298A/F305A/T395A/F396A.

B Immunoprecipitation (IP) of wild-type and mutant FLAG-LSM14A proteins from benzonase-treated HeLa cell extracts using anti-FLAG antibody. Immunoprecipitated complexes were separated by SDS–PAGE and probed with antibodies against indicated proteins.

C Confocal fluorescence micrographs of fixed HeLa cells expressing FLAG-tagged wild-type or mutant LSM14. Cells were stained with anti-FLAG (green) and anti-DDX6 (red) antibodies. The merged images show the FLAG signal in green and the DDX6 signal in red.

Source data are available online for this figure.

dispensable for the interaction with DDX6_C (Figs 3C and 5A). Taken together, these results confirm that a stable LSM14–DDX6 interaction is dependent on interactions involving all invariant phenylalanine residues in both the LSM14 FDF and TFG motifs.

The integrity of the DDX6 interaction motif in LSM14 is required for *de novo* P-body assembly

LSM14 and DDX6 localize both to P-bodies and stress granules (Yang *et al*, 2006). To determine whether the TFG motif is critical for LSM14 localization, we used immunofluorescence microscopy to examine the subcellular localization of FLAG-tagged wild-type and mutant LSM14 proteins in HeLa cells depleted of endogenous LSM14. FLAG-LSM14 localized to endogenous P-bodies, as judged by co-localization with DDX6 (Fig 5C) and with DCP1 (Fig EV2A). In contrast, LSM14 proteins lacking the TFG motif, or harboring an alanine substitution of Phe396 in the TFG motif, were unable to localize to P-bodies. Indeed, P-body formation was disrupted in both cases, as indicated by the loss of DCP1 localization, suggesting that the interaction between LSM14 and DDX6 is required for *de novo* P-body formation (Figs 5C and EV2A). Notwithstanding these LSM14 variants being unable to promote P-body formation, they still localized to stress granules in arsenite-treated cells, based on observed co-localization with the stress granule marker HUR (Fig EV2B). Taken together, these data demonstrate that LSM14 promotes P-body formation *in vivo*, at least in part, by utilizing its TFG motif to interact with DDX6.

The LSM14 FFD motif recruits the decapping activator EDC4

Our structural observations and biochemical experiments indicate that LSM14 relies on both its FDF and TFG motifs to bind DDX6. The two motifs are interspaced by an unstructured sequence containing the FFD motif, whose sequence is largely conserved from yeast to humans, pointing to its functional significance (Fig 4A). Interestingly, although the FFD motif does not bind DDX6, a LSM14 protein lacking the FFD motif did not promote the formation of P-bodies (Fig 5C). Short linear motifs (SLIMs), such as the FFD motif, often serve as protein interaction platforms (Jonas & Izaurralde, 2013). We therefore hypothesized that the LSM14 FFD motif mediates interactions with additional mRNA silencing factors to promote P-body assembly. To test this hypothesis, we set out to characterize the interactomes for both wild-type LSM14 and LSM14 lacking the FFD motif (LSM14_{ΔFFD}). To this end, FLAG-tagged LSM14 and LSM14_{ΔFFD} proteins were expressed in HeLa cells and immunoprecipitated from benzonase-treated cell lysates; LSM14-bound proteins were subsequently trypsinized and analyzed by mass spectrometry (Fig 6A). WT LSM14 co-precipitated with a number of previously identified P-body components, including 4E-T, DDX6, and PATL1. We also identified PRMT1, an arginine methyltransferase previously reported to interact with LSM14 (Matsumoto *et al*, 2012), and C1QBP, a mitochondrial protein that has recently been identified to associate with DDX6 (Zhang *et al*, 2013). Interestingly, LSM14 also co-precipitated EDC4, an enhancer of mRNA decapping not previously reported to associate with LSM14. LSM14_{ΔFFD} also efficiently co-precipitated 4E-T, DDX6, PATL1, PRMT1, and C1QBP. However, interaction with EDC4 was markedly reduced (Fig 6A). Mass spectrometry

data were subsequently corroborated by co-immunoprecipitation experiments followed by Western blotting using an EDC4-specific antibody (Fig 6B). In addition, a mutant LSM14 protein in which four conserved aromatic residues in the FFD motif (Tyr362^{LSM14}, Tyr363^{LSM14}, Phe369^{LSM14}, and Phe370^{LSM14}; FFD_{MUT}) were substituted with alanines did not co-precipitate EDC4, while interactions with 4E-T, PATL1, and DDX6 remained unperturbed (Fig 6B). Together, these results suggest that human LSM14 uses its evolutionarily conserved FFD motif as an interaction hotspot to recruit EDC4.

LSM14 engages known interaction hotspots on DDX6 with unique mode of binding

Comparison of the LSM14_{FDF-TFG}–DDX6_C complex structure with the structures of DDX6 bound to the decapping activator and translational repressor proteins EDC3 and 4E-T, as well as the structure of the yeast Pat1–Dhh1 complex, reveals that they all interact with the same three hydrophobic pockets on the C-terminal RecA domain of DDX6 (Fig EV3A). EDC3 and Pat1 contain FDF motifs similar to that found in LSM14, whereas in 4E-T, the FDF motif is replaced by an equivalent IEL (Ile-Glu-Leu) motif (Fig EV3B). All four proteins use their FDF or IEL motifs to occupy one of the DDX6_C hydrophobic pockets. Additionally, LSM14 and EDC3 contain a helical element downstream of the FDF motif that is anchored on the surface of DDX6_C by the insertion of a conserved phenylalanine (Phe305^{LSM14}, Phe199^{EDC3}) into the second hydrophobic patch. This additional α -helix, however, is absent in Pat1 and 4E-T. The third hydrophobic interaction hotspot on DDX6_C is occupied by the TFG motifs of LSM14, Pat1 and the related WFS (tryptophan-phenylalanine-serine) motif of 4E-T. The central phenylalanine, common to the TFG and WFS motifs, is fixed in the third hydrophobic pocket of DDX6_C, and binding is reinforced by additional hydrogen-bonding interactions of neighboring residues (Figs 4C and EV3A; Tritschler *et al*, 2009; Sharif *et al*, 2013; Ozgur *et al*, 2015). EDC3, PATL1, and 4E-T harbor their TFG/WFS motifs immediately upstream of the FDF motif. In contrast, the two DDX6-interacting motifs in LSM14 are non-contiguous and adopt an inverted arrangement, with the TFG motif being placed downstream of the FDF motif in the polypeptide sequence of LSM14. Although the specific details of these interactions vary from one factor to another, these observations nevertheless collectively suggest that the binding of these factors to DDX6 is mutually exclusive (Fig EV3B).

To address whether the unique binding mode observed for LSM14 is reflected in the affinity of LSM14_{FDF-TFG} for DDX6_C as compared to PATL1_{TFG-FDF}, EDC3_{TFG-FDF}, and 4E-T_{WFS-IEL}, we performed ITC experiments. LSM14_{FDF-TFG} bound DDX6_C with an equilibrium dissociation constant of 1.6 μ M, whereas PATL1_{TFG-FDF}, EDC3_{TFG-FDF}, and 4E-T_{WFS-IEL} bound DDX6_C with K_d values of 0.23, 0.31, and 0.39 μ M, respectively (Table 2 and Fig EV4). These measurements thus suggest that despite their overall high structural similarity, LSM14 exhibits a unique binding mode for the C-terminal RecA domain of DDX6, which may be a consequence of the unique function of the FFD motif in mediating EDC4 interaction. Nevertheless, the affinities of the DDX6-interacting motifs in LSM14, PATL1, EDC3, and 4E-T all fall within an order of magnitude of one another, suggesting that these proteins engage DDX6_C in a mutually competitive manner.

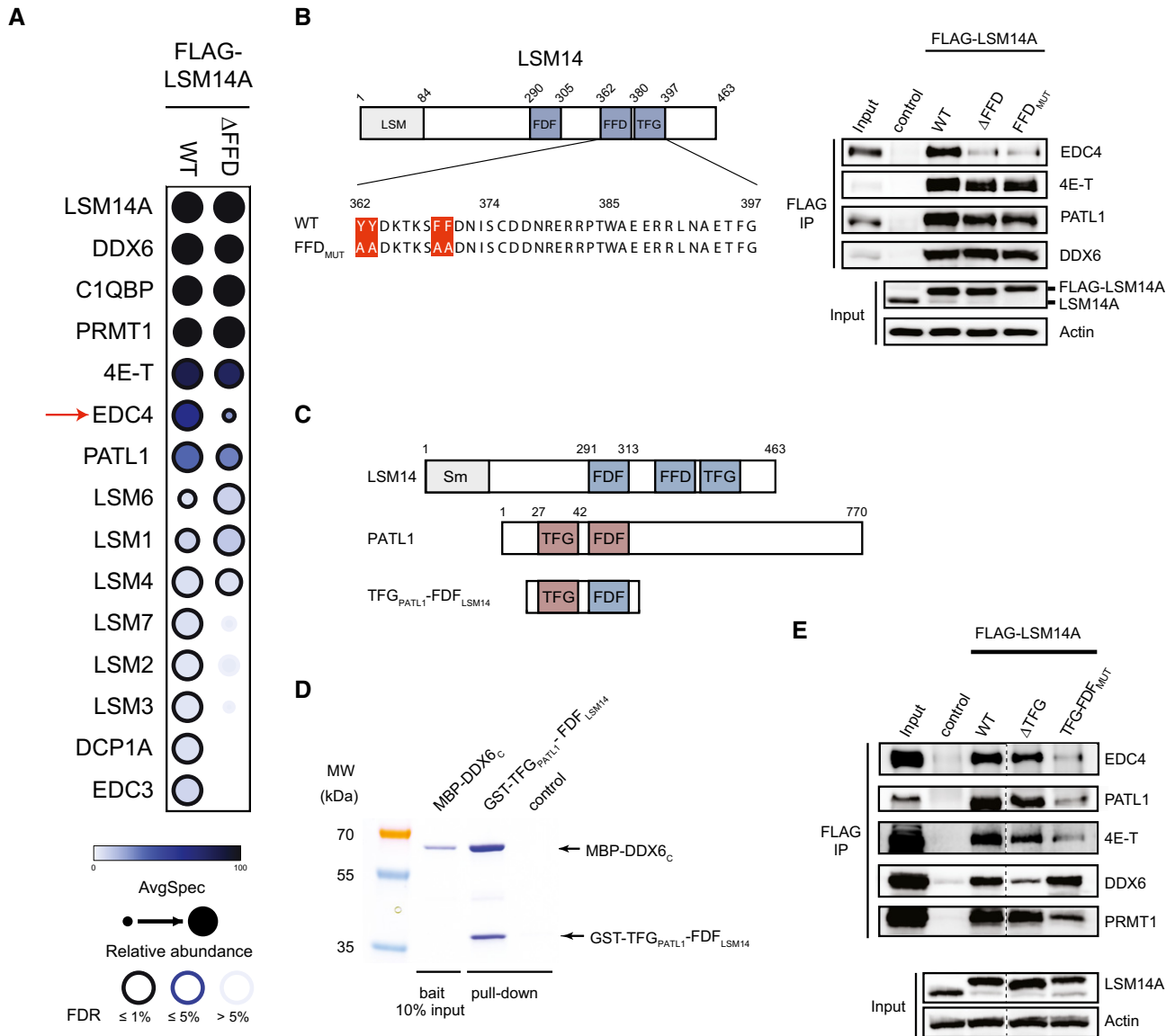


Figure 6. LSM14 motifs support formation of protein interaction network including EDC4.

- A Dot plot depicting high-confidence protein interactions identified by affinity purification of FLAG-LSM14 and FLAG-LSM14 Δ FFD in HeLa cells. An average of two independent experiments for each tagged variant is presented. Node color represents the absolute spectral count sum, the node edge color corresponds to the SAINTexpress Bayesian FDR value (BFDR), and the node size displays the relative abundance of a given prey comparing FLAG-LSM14 to FLAG-LSM14 Δ FFD samples. Avg-Spec denotes the spectral counts for each indicated prey. Reduction of EDC4 interaction in FLAG-LSM14 Δ FFD is indicated with red arrow.
- B Left: Schematic representation of wild-type and FFD mutant (FFD $_{MUT}$). Right: Immunoprecipitation (IP) of WT, Δ FFD, and FFD $_{MUT}$ FLAG-LSM14A proteins from benzoylase-treated HeLa cell extracts using anti-FLAG antibody. Immunoprecipitated complexes were separated by SDS-PAGE and probed by Western blotting using antibodies against the indicated proteins.
- C Schematic diagram of LSM14 and PATL1 proteins, as well as the TFG $_{PATL1}$ -FDF $_{LSM14}$ construct in which the PATL1 TFG motif (residues 27–42) has been fused upstream to the LSM14 FDF motif (residues 291–313).
- D SDS-PAGE analysis of a pull-down experiment using recombinant MBP-DDX6 $_C$ protein immobilized on amylose-beads and incubated with recombinant GST-TFG $_{PATL1}$ -FDF $_{LSM14}$ protein construct.
- E Immunoprecipitation (IP) of WT, Δ TFG, and TFG-FDF $_{MUT}$ FLAG-LSM14A constructs. In the TFG-FDF $_{MUT}$ construct, the LSM14 TFG motif has been deleted and the equivalent motif from PATL1 was placed upstream of the FDF motif. Proteins were precipitated from benzoylase-treated HeLa cell extracts using anti-FLAG antibody, separated by SDS-PAGE and probed with antibodies against the indicated proteins.

Source data are available online for this figure.

Topology of DDX6-binding motifs in LSM14 is required for LSM14 protein complex assembly

We hypothesized that the inverted arrangement of the FDF and TFG motifs in LSM14 is required to support the LSM14–EDC4 interaction.

To test this hypothesis, we first fused the LSM14 FDF motif downstream of the “upstream” TFG motif from human PATL1 and verified that the resulting construct (TFG $_{PATL1}$ -FDF $_{LSM14}$) was capable of binding to DDX6 $_C$ in a pull-down assay (Figs 6C and D, and EV3C). Interestingly, the TFG $_{PATL1}$ -FDF $_{LSM14}$ construct has the highest

affinity for DDX6_C, with a K_d of 40 nM, as determined by ITC (Table 2 and Fig EV4). This is comparable to the affinity of yeast Pat1 (32 nM), which contains an endogenous tandem TFG-FDF motif, for the yeast DDX6 homolog Dhh1 (Sharif *et al*, 2013). Next, we inserted the PATL1 TFG motif upstream of the FDF in an LSM14 construct lacking the endogenous TFG motif (TFG-FDF_{MUT}). The resulting protein indeed bound DDX6 as well as wild-type LSM14 in co-immunoprecipitation assays. However, interactions with 4E-T, PATL1, PRMT1, and EDC4 were impaired (Fig 6E). Moreover, this mutant was unable to induce P-body formation *in vivo* (Fig EV2C). Taken together, these data suggest that the unique mode by which the conserved motifs in LSM14 contact DDX6 allows for LSM14 to form higher-order protein complexes with 4E-T, PATL1, PRMT1, and EDC4 and facilitate P-body assembly.

Discussion

We previously showed that LSM14 utilizes its N-terminal LSM domain to directly bind to 4E-T. Here we present the crystal structure of the LSM domain of human LSM14 in complex with a C-terminal LSM14-interacting fragment of 4E-T. Our structure shows that the 4E-T C-terminus contains a bi-partite interaction motif that contacts both faces of the LSM domain by wrapping around it. The amino acid residues that contact LSM14 are phylogenetically conserved in 4E-T proteins, including the *D. melanogaster* 4E-T homolog. Moreover, LSM14 residues on the surface of the LSM domain that contact 4E-T are also highly conserved in the *D. melanogaster* LSM14 homolog Trailer hitch (Tral), implying broad conservation of the LSM14–4E-T interaction in metazoans. Our previous work showed that in addition to the C-terminal 4E-T fragment, the middle region of 4E-T (residues 335–490) also interacts with the LSM domain of LSM14 *in vitro* (Nishimura *et al*, 2015). This finding was recently corroborated by other studies demonstrating the middle region to be sufficient for this interaction (Kamenska *et al*, 2016). The middle and C-terminal regions contain conserved hydrophobic residues that can be partially aligned (Fig EV1A). Given that mutations in the hydrophobic interaction surfaces on the LSM14 LSM domain completely disrupt 4E-T binding *in vivo*, we conclude that the middle and C-terminal 4E-T regions bind to the LSM domain in a highly similar, and likely mutually exclusive manner. Moreover, these results suggest that the two 4E-T motifs are functionally redundant and serve either to promote LSM14 binding through increased avidity or to facilitate LSM14 binding with a 1:2 stoichiometry.

Although the C-terminal fragment of 4E-T directly binds LSM14, we previously showed that it is unable to interact with EDC3 (Nishimura *et al*, 2015). Similarly, the *D. melanogaster* translational repressor protein CUP, a paralog of 4E-T, interacts with Tral but not with EDC3 (Tritschler *et al*, 2008). Our structure of the LSM14_{LSM}–4E-T_C complex provides clues to explain the inability of EDC3 to bind 4E-T. Structural comparison of the LSM14 and EDC3 LSM domains indicates that EDC3 contains additional hydrophobic residues in the N-terminal region (Trp5^{EDC3}) and in the loop connecting strands β 1 and β 2 (Leu18^{EDC3}) that cap the hydrophobic pockets in its LSM domain, which would preclude 4E-T association by steric clashes (Fig EV5A and B). Thus, despite being structurally quite similar, the LSM domains of EDC3 and LSM14 have diverged to

interact with distinct binding partners. EDC3 proteins interact with the DCP1–DCP2 decapping machinery (Tritschler *et al*, 2008; Fromm *et al*, 2012), whereas LSM14-containing complexes have been proposed to repress mRNA translation in the absence of decapping (Jonas & Izaurralde, 2013). The distinct structural features of EDC3 and LSM14 proteins thus underpin their functional divergence. Although the *D. melanogaster* LSM14 ortholog Tral was previously reported to interact with DCP1 via its N-terminal LSM domain (Tritschler *et al*, 2008), our proteomic analysis of the human LSM14 interactome suggests that DCP1 only weakly or indirectly associates with human LSM14 (Fig 6A). Thus, human and *Drosophila* LSM14 orthologs may not directly interact with the same partners. In keeping with this possibility, Tral is not essential for P-body formation, whereas human LSM14 is (Yang *et al*, 2006; Eulalio *et al*, 2007b). Interestingly, while LSM14 is a component of both P-bodies and stress granules, 4E-T is generally only found in P-bodies. Whether the LSM domain of LSM14 associates with other binding partners when it localizes to stress granules remains to be investigated.

DDX6 plays an important role in mRNA gene silencing by repressing translation and enhancing mRNA decapping and decay. A number of decapping and translational repression factors, including EDC3, 4E-T, PATL1, and LSM14 contain an FDF motif, or a variant thereof, and interact with hydrophobic surfaces on the C-terminal RecA domain of DDX6. Due to having overlapping binding sites on DDX6, these factors are likely to bind to DDX6 in a mutually exclusive and therefore competitive manner (Ozgur *et al*, 2015). The FDF motif in LSM14 has previously been reported to co-immunoprecipitate DDX6_C, albeit less efficiently than full-length LSM14 (Tritschler *et al*, 2009). Our biochemical and structural data indicate that LSM14 employs a bipartite binding mode to interact with DDX6, with both the FDF and TFG making extensive interactions with the DDX6 C-terminal RecA domain. Importantly, both the FDF and TFG motifs are essential for stable interaction with DDX6, both *in vitro* and *in vivo*. Although LSM14 contacts the same hydrophobic surfaces on DDX6 as EDC3, 4E-T, and PATL1, our crystal structure shows that the LSM14 binding mode is unique. Unlike in EDC3 and PATL1, which maintain a TFG motif upstream and proximal to their FDF motif, the two motifs have an inverted arrangement in LSM14, with the TFG motif located downstream and distal to the FDF motif. Our ITC assays indicate that LSM14 binds to DDX6 with weaker affinity than EDC3, 4E-T, and PATL1. Nevertheless, a substantial fraction of DDX6 is likely to be bound by LSM14 *in vivo*, considering the relative cellular abundance of these factors. Recent quantitative proteomic studies have shown that the cellular concentration of DDX6 in HeLa cells (~550 nM) is approximately equal to or higher than the combined concentrations of LSM14A and LSM14B proteins (235 and 94 nM, respectively), 4E-T (10 nM), EDC3 (93 nM), and PATL1 (100 nM; Hein *et al*, 2015); DDX6 is thus sufficiently abundant to accommodate all of its known interaction partners. However, direct interactions with DDX6 are also likely to be modulated by indirect interactions, for example, between LSM14 and 4E-T. Moreover, the interactions are also influenced by the propensity of DDX6 and many of its interacting partners to undergo phase separation by liquid droplet formation, which in turn may have an effect on their local concentrations (Schutz *et al*, 2017). Although the spatial and temporal interplay of DDX6 interactions is still incompletely understood, these insights nevertheless underscore the

critical importance of DDX6 in acting as a protein–protein interaction hub that engenders distinct functional outcomes in its target mRNAs depending on the recruitment of specific interaction partners.

Why does LSM14 utilize a non-canonical binding mechanism as compared to other DDX6-interacting proteins? In LSM14, the FDF and TFG motifs are interspaced by a flexible low-complexity region containing an FFD motif that is conserved from yeast to humans. Our proteomic analysis reveals that human LSM14 also interacts with the decapping enhancer protein EDC4, and that this interaction is dependent on the presence of the FFD motif. EDC4 has been reported to directly bind the DCP1–DCP2 decapping complex and the 5′–3′ exoribonuclease XRN1 (Chang *et al.*, 2014). It is likely that LSM14 recruits these enzymes via EDC4 as our mass spectrometry data showed that although the association of LSM14 with DCP1, DCP2, and XRN1 was low compared to EDC4, this was further reduced upon deleting the FFD motif in LSM14. Surprisingly, our data also illustrate that a LSM14 protein construct in which the TFG motif is placed upstream of the FDF motif can effectively bind to DDX6. However, this protein is unable to efficiently bind other interacting partners, including 4E-T, PATL1, EDC4, and PRMT1. Taken together, these observations suggest that LSM14 may have adopted its unique mode of binding to DDX6 in order to recruit EDC4 to form higher-order protein complexes that elicit mRNA silencing.

LSM14 proteins are highly conserved in eukaryotes. Interestingly, both the LSM domain and the FFD motif are highly conserved between yeast SCD6 and human LSM14. However, the interactions shown in our study to be mediated by these motifs cannot be extended to the yeast homolog SCD6 because their respective interaction partners (4E-T and EDC4) are both absent in yeast. It would be important to elucidate the protein interactions mediated by these regions in SCD6. It should also be noted that a recent study showed that SCD6 efficiently interacts with eIF4G1 in a manner dependent on Hmt1-mediated methylation of the SCD6 RGG motif, and that this is required to induce translational repression (Poornima *et al.*, 2016). Although we detected interaction between human LSM14 and the protein arginine methyl transferase PRMT1, consistent with previously reported methylation of the LSM14 RGG motif (Matsumoto *et al.*, 2012), we failed to detect eIF4G binding by mass spectrometry. These differences in the interaction networks centered on human LSM14 and yeast SCD6 allude to a divergence in their mechanism of mRNA silencing that remains to be elucidated.

Materials and Methods

Expression and purification of recombinant proteins

The C-terminal RecA domain of human DDX6 spanning residues 303–469 (DDX6_C) was expressed as a fusion protein containing an N-terminal hexahistidine (His₆) affinity tag and the maltose binding protein (MBP) polypeptide sequence followed by the tobacco etch virus (TEV) protease cleavage site. The DDX6-interacting fragment of *C. elegans* LSM14 spanning residues 184–268 (corresponding residues for human protein: 290–397, CeLSM14_{FDF-TFG}) was expressed as a fusion protein with an N-terminal glutathione S-transferase (GST) affinity tag followed by the human rhinovirus 3C protease

cleavage site. The N-terminal LSM domain of human LSM14 spanning residues 1–84 (LSM14_{LSM}) was expressed with an N-terminal hexahistidine (His₆) affinity tag and the maltose binding protein (MBP) polypeptide sequence followed by the tobacco etch virus (TEV) protease cleavage site. The C-terminal motif from human 4E-T spanning residues 954–985 (4E-T_C) was expressed fused to an N-terminal glutathione S-transferase (GST) affinity tag followed by the human rhinovirus 3C protease cleavage site.

Recombinant proteins were expressed individually in *Escherichia coli* BL21 (DE3) Rosetta 2 (Novagen) cells at 18°C for 16 h (overnight). Cells were lysed by sonication in lysis buffer (20 mM Tris pH 8.0, 250 mM KCl) supplemented with 10 mM imidazole pH 8.0 for His₆-tagged proteins or 1 mM DTT for GST-tagged proteins, respectively. For purification of His₆-tagged proteins, the cleared lysate was applied to a 5 ml Ni-NTA Superflow cartridge (Qiagen) and the column was washed with lysis buffer supplemented with 50 mM imidazole. Bound proteins were eluted using lysis buffer supplemented with 250 mM imidazole and dialyzed against lysis buffer in the presence of TEV protease at 4°C for 16 h to cleave the His₆-MBP affinity tag. To remove the cleaved affinity tag, DDX6_C was subjected to cation exchange chromatography on a 5 ml HiTrap Heparin HP column (GE Healthcare), eluting with a salt gradient. To remove the cleaved His₆-MBP affinity tag from LSM14_{LSM}, the protein was reappplied to a 5 ml Ni-NTA Superflow cartridge and the flow-through fraction was collected. Target proteins were further purified by size exclusion chromatography using a Superdex 75 16/600 column (GE Healthcare) in 20 mM Tris pH 7.5, 250 mM KCl, 1 mM DTT. For purification of GST-tagged proteins, the cleared lysate was applied to a 5 ml Glutathione Sepharose 4B cartridge (GE Healthcare). Bound proteins were eluted using lysis buffer supplemented with 10 mM reduced glutathione and subsequently dialyzed against lysis buffer in the presence of 3C protease for 16 h at 4°C to cleave the GST affinity tag. The GST tag was removed by reapplying the cleaved proteins onto a 5 ml Glutathione Sepharose 4B cartridge (GE Healthcare). The proteins were further purified by size exclusion chromatography using a Superdex 75 16/600 column (GE Healthcare) in 20 mM Tris pH 7.5, 250 mM KCl, 1 mM DTT.

Glutathione S-transferase- and MBP-fused fragments of human DDX6_C, LSM14, and 4E-T used in pull-down experiments were expressed and purified as described above, except that the dialysis and cleavage step was omitted. Amino acid substitutions were introduced by QuikChange site-directed mutagenesis and verified by DNA sequencing. For selenomethionine (SeMet) labeling of the 4E-T_C^{V963M} point mutant, expression was carried out in M9 minimal medium supplemented with 1 μg ml⁻¹ biotin and 1 μg ml⁻¹ thiamine. Bacteria were grown to OD₆₀₀ of 0.8 followed by the addition of an amino acid mix (0.1 mg ml⁻¹ Lys, Thr, Phe and 0.05 mg ml⁻¹ Leu, Ile, Val, SeMet) allowing the incorporation of SeMet. After 30 min, the temperature was reduced to 18°C and expression was induced by addition of 200 μM isopropyl-β-D-thiogalactopyranoside (IPTG). Purification of SeMet labeled protein was performed as described above. Protein complexes for crystallization were formed by incubating LSM14_{FDF-TFG} with DDX6_C and LSM14_{LSM} with 4E-T_C, both with a molar ratio of 1:1.5. Reconstituted complexes were subjected to size exclusion chromatography using a Superdex 75 16/600 column (GE Healthcare) in 20 mM Tris pH 7.5, 250 mM KCl, 1 mM DTT.

Crystallization and structure determination

LSM14_{LSM}-4E-T_C complex

The structure of the LSM14_{LSM}-4E-T_C complex was determined by a single-wavelength anomalous diffraction (SAD) experiment, exploiting the anomalous diffraction properties of selenomethionine (SeMet)-substituted 4E-T_C^{V963M} protein. The complex of LSM14_{LSM} and SeMet 4E-T_C^{V963M} variant was concentrated to 12 mg ml⁻¹ and crystallized at 4°C using a reservoir solution containing 2 M (NH₄)₂SO₄, 2% PEG400, 0.1 M HEPES pH 7. For cryoprotection, crystals were transferred into 2 M (NH₄)₂SO₄, 2% PEG400, 0.1 M HEPES pH 7, 15% ethylene glycol and frozen in liquid nitrogen. X-ray diffraction data were collected at beam line X06DA (PXIII) of the Swiss Light Source (Paul Scherrer Institute, Villigen, Switzerland). The crystals diffracted to a resolution of 2.6 Å, belonged to space group *P*4₂1₂ and contained two copies of the complex per asymmetric unit. Two data sets were collected by exposing different parts of the same crystal and rotating the crystal through 360°. Data were processed using XDS (Kabsch, 2010). Localization of selenium sites, phasing, density modification, and automated building of a preliminary model was carried out using the AutoSol (Adams *et al*, 2010) routine implemented in Phenix. The initial atomic model was completed by manual building using COOT (Emsley & Cowtan, 2004) and refined using Phenix.Refine (Afonine *et al*, 2012).

CeLSM14_{FDF-TFG}-DDX6_C complex

Purified CeLSM14_{FDF-TFG}-DDX6_C complex was concentrated to 15 mg ml⁻¹. Crystallization was carried out using the hanging drop vapor diffusion method at 20°C by mixing equal volumes (1 + 1 μl) of the complex and a reservoir solution containing 1.55 M Li₂SO₄ and 0.1 M HEPES pH 7.5. For cryoprotection, crystals were transferred into 1.55 M Li₂SO₄, 0.1 M HEPES pH 7.5, 10% ethylene glycol and flash cooled in liquid nitrogen. X-ray diffraction data were collected at beam line X06DA (PXIII) of the Swiss Light Source (Paul Scherrer Institute, Villigen, Switzerland) to a resolution of 3.0 Å and processed using XDS (Kabsch, 2010). The structure was solved by molecular replacement with Phenix.Phaser (McCoy *et al*, 2007) using a previously published structure of the C-terminal RecA domain from DDX6 (PDB ID 2WAY; Tritschler *et al*, 2009) as a search model. In addition to human DDX6_C, readily interpretable electron density corresponding to CeLSM14_{FDF-TFG} could be observed and was built manually. The atomic model of the DDX6_C-CeLSM14_{FDF-TFG} complex was completed by iterative building and refinement in COOT (Emsley & Cowtan, 2004) and PHENIX.Refine (Afonine *et al*, 2012), respectively.

Isothermal titration calorimetry

Recombinant proteins used for ITC experiments were purified as described above with a final size exclusion chromatography step (Superdex 75 16/600 column, GE Healthcare) using the same buffer (20 mM Tris pH 7.5, 150 mM KCl) for all proteins. ITC experiments were performed at 20°C using a MicroCal iTC200 (GE Healthcare). Purified interaction motifs from LSM14, PATL1, EDC3, and 4E-T (500 μM) were injected 30 times in 1.2-μl aliquots into the sample cell containing 300 μl of LSM14_{LSM} or DDX6_C (50 μM). Data were fit to a single-binding site model using the Origin version 7.0 software

(MicroCal), yielding the enthalpy (ΔH), entropy (ΔS), and the dissociation constant (K_d) of the reaction.

Cell culture and stable cell line generation

HeLa cells were incubated at 37°C at 5% CO₂, in DMEM (Wisent) supplemented with 10% fetal bovine serum (FBS; Wisent) and 1% penicillin/streptomycin (Wisent). VSV-G pseudotyped pBABE-3FLAG-LSM14A retroviruses and a pLKO.1-blast lentivirus expressing a short hairpin RNA (shRNA) targeting human LSM14 (5'-GGTA CAGAAGACAGACCGACA-3') were produced in HEK293T cells. HeLa cells were subsequently transduced and selected with puromycin (1 μg ml⁻¹) and blasticidin (8 μg ml⁻¹).

Co-immunoprecipitation and mass spectrometry analysis

For co-immunoprecipitation (Co-IP) experiments, HeLa cells stably expressing 3x-FLAG-LSM14A proteins were pelleted, frozen on dry ice, and resuspended in lysis buffer equal to four times the pellet volume (50 mM HEPES pH 7.5, 100 mM KCl, 2 mM EDTA, 10% glycerol, 1 mM DTT, and 0.1% NP-40) supplemented with protease inhibitors. Lysates were clarified by centrifugation at 20,000 *g* for 20 min at 4°C. Lysates were pre-cleared with 30 μl of packed Protein G Agarose Fast Flow (Millipore) for 1 h at 4°C with end-over-end rotation. Lysates were adjusted to a final concentration of 2 mg ml⁻¹ and incubated with benzonase (1 μl ml⁻¹ of lysate, Millipore) and 20 μl of packed FLAG M2 agarose (Sigma-Aldrich) at 4°C for 3.5 h with end-over-end rotation. The beads were then washed five times with 1 ml of cold lysis buffer and eluted by heating with 40 μl of 1× SDS-PAGE loading buffer. Proteins were separated by SDS-PAGE followed by Western blotting. Co-immunoprecipitation experiments prepared for mass spectrometry-based analysis were performed essentially as described above using 1.2 mg of lysate per Co-IP, followed by three washes in lysis buffer and two washes in 50 mM ammonium bicarbonate pH 8.0. Samples were then analyzed by mass spectrometry as previously described (Kean *et al*, 2012).

λN-BoxB reporter tethering assay

HeLa cells were transiently transfected using PEI reagent (Polysciences) with 20 ng of RL (Renilla luciferase)-5BoxB plasmid, 20 ng of control FL (Firefly luciferase) plasmid, and varying amounts of plasmids expressing λNHA-tagged proteins to obtain equal expression, as determined by SDS-PAGE and analyzed by Western blotting, as described previously (Zipprich *et al*, 2009; Fabian *et al*, 2011). Construct expressing the silencing domain of the human GW182 served as a positive control (Zipprich *et al*, 2009; Fabian *et al*, 2011). Twenty-four hours post-transfection, 20% of the cells were lysed in Passive Lysis Buffer (Promega), and luciferase activity was determined using the Dual Luciferase Reporter Assay System kit. All experiments were performed in triplicate.

Antibodies

Rabbit polyclonal antibodies against PATL1 (A303-482A), DDX6 (A300-460A), and EDC4 (A300-745A) were from Bethyl laboratories, and LSM14 (ABE37) was from Millipore. Mouse monoclonal

antibodies against β -actin and FLAG were from Sigma. Rabbit polyclonal antibody against 4E-T was from Abcam (ab55881).

Pull-down experiments

For MBP pull-down experiments, 10 μ g of MBP-tagged DDX6_C or LSM14_{LSM} was immobilized on 50 μ l (50% slurry) of amylose resin (NEB) in a binding buffer containing 20 mM Tris pH 7.5, 150 mM KCl, 1 mM DTT, and 0.1% Tween-20. The beads were washed and incubated with 15 μ g of the respective GST-tagged proteins in binding buffer for 1 h at 4°C with gentle rocking. Subsequently, the beads were washed four times with 1 ml of binding buffer and proteins were eluted by boiling the resin with 20 μ l of SDS-PAGE sample buffer. Proteins were analyzed by SDS-PAGE and visualized by Coomassie staining.

SEC-MALS analysis of the LSM14_{LSM}-4E-T_C complex

To verify the stoichiometry of the LSM14_{LSM} and 4E-T_C^{V963M} complex, size exclusion chromatography combined with multi-angle light scattering was performed. 100 μ l of purified protein complex at a concentration of 1 mg ml⁻¹ was injected onto a Superdex 75 10/300 column (GE Healthcare) and eluted with 250 mM KCl, 20 mM Tris pH 7.5, 1 mM DTT, and the light scattering of eluted proteins was recorded downstream using a miniDAWN MALS detector (Wyatt Technology). Data recording and analysis was performed using ASTRA (Wyatt Technology).

Data availability

The atomic coordinates and structure factors reported in this study have been deposited in the Protein Data Bank (PDB) under accession codes 6F9W (LSM14_{LSM}-4E-T_C complex) and 6F9S (DDX6_C-LSM14_{FDF-TFG} complex).

Expanded View for this article is available online.

Acknowledgements

We thank Meitian Wang, Vincent Olieric, and Takashi Tomizaki at the Swiss Light Source (Paul Scherrer Institute, Villigen, Switzerland) for assistance with X-ray diffraction measurements. We are grateful to Daniel Bojar and Pawel Sledz for preliminary work on the project. This work was supported by an European Research Council (ERC) Starting Grant ANTIVIRNA (Grant no. ERC-StG-337284) to M.J., a Canadian Institutes of Health Research (CIHR) grant to M.R.F. (MOP-130425), a Natural Sciences and Engineering Research Council of Canada (NSERC) Discovery grant to M.R.F. (RGPIN-2015-03712), and an NSERC Discovery and Accelerator Supplement to A.C.G. (RGPIN-2014-06434 and RGPAS 462169). M.R.F. is a recipient of the Fonds de recherche du Québec-Santé (FRQS) Chercheur-Boursier Junior 1 and CIHR New Investigator awards. M.J. is International Research Scholar of the Howard Hughes Medical Institute and Vallee Scholar of the Bert L & N Kuggie Vallee Foundation.

Author contributions

TB, HF, ZP, J-YY, A-CG, MRF, and MJ designed research; TB, HF, ZP, and J-YY performed experiments; TB, HF, MRF, and MJ wrote the manuscript.

Conflict of interest

The authors declare that they have no conflict of interest.

References

- Adams PD, Afonine PV, Bunkoczi G, Chen VB, Davis IW, Echols N, Headd JJ, Hung LW, Kapral GJ, Grosse-Kunstleve RW, McCoy AJ, Moriarty NW, Oeffner R, Read RJ, Richardson DC, Richardson JS, Terwilliger TC, Zwart PH (2010) PHENIX: a comprehensive Python-based system for macromolecular structure solution. *Acta Crystallogr D Biol Crystallogr* 66: 213–221
- Afonine PV, Grosse-Kunstleve RW, Echols N, Headd JJ, Moriarty NW, Mustyakimov M, Terwilliger TC, Urzhumtsev A, Zwart PH, Adams PD (2012) Towards automated crystallographic structure refinement with phenix.refine. *Acta Crystallogr D Biol Crystallogr* 68: 352–367
- Albrecht M, Lengauer T (2004) Novel Sm-like proteins with long C-terminal tails and associated methyltransferases. *FEBS Lett* 569: 18–26
- Arribas-Layton M, Wu D, Lykke-Andersen J, Song H (2013) Structural and functional control of the eukaryotic mRNA decapping machinery. *Biochem Biophys Acta* 1829: 580–589
- Carroll JS, Munchel SE, Weis K (2011) The DExD/H box ATPase Dhh1 functions in translational repression, mRNA decay, and processing body dynamics. *J Cell Biol* 194: 527–537
- Chang CT, Bercovich N, Loh B, Jonas S, Izaurralde E (2014) The activation of the decapping enzyme DCP2 by DCP1 occurs on the EDC4 scaffold and involves a conserved loop in DCP1. *Nucleic Acids Res* 42: 5217–5233
- Chen CY, Shyu AB (2011) Mechanisms of deadenylation-dependent decay. *Wiley Interdiscip Rev RNA* 2: 167–183
- Chowdhury A, Tharun S (2009) Activation of decapping involves binding of the mRNA and facilitation of the post-binding steps by the Lsm1-7-Pat1 complex. *RNA* 15: 1837–1848
- Coller J, Parker R (2005) General translational repression by activators of mRNA decapping. *Cell* 122: 875–886
- Emsley P, Cowtan K (2004) Coot: model-building tools for molecular graphics. *Acta Crystallogr D Biol Crystallogr* 60: 2126–2132
- Eulalio A, Behm-Ansmant I, Izaurralde E (2007a) P bodies: at the crossroads of post-transcriptional pathways. *Nat Rev Mol Cell Biol* 8: 9–22
- Eulalio A, Behm-Ansmant I, Schweizer D, Izaurralde E (2007b) P-body formation is a consequence, not the cause, of RNA-mediated gene silencing. *Mol Cell Biol* 27: 3970–3981
- Fabian MR, Cieplak MK, Frank F, Morita M, Green J, Srikumar T, Nagar B, Yamamoto T, Raught B, Duchaine TF, Sonenberg N (2011) miRNA-mediated deadenylation is orchestrated by GW182 through two conserved motifs that interact with CCR4-NOT. *Nat Struct Mol Biol* 18: 1211–1217
- Fromm SA, Truffault V, Kamenz J, Braun JE, Hoffmann NA, Izaurralde E, Sprangers R (2012) The structural basis of Edc3- and Scd6-mediated activation of the Dcp1:Dcp2 mRNA decapping complex. *EMBO J* 31: 279–290
- Hein MY, Hubner NC, Poser I, Cox J, Nagaraj N, Toyoda Y, Gak IA, Weisswange I, Mansfeld J, Buchholz F, Hyman AA, Mann M (2015) A human interactome in three quantitative dimensions organized by stoichiometries and abundances. *Cell* 163: 712–723
- Holm L, Laakso LM (2016) Dali server update. *Nucleic Acids Res* 44: W351–W355
- Jonas S, Izaurralde E (2013) The role of disordered protein regions in the assembly of decapping complexes and RNP granules. *Genes Dev* 27: 2628–2641
- Kabsch W (2010) XDS. *Acta Crystallogr D Biol Crystallogr* 66: 125–132
- Kambach C, Walke S, Young R, Avis JM, de la Fortelle E, Raker VA, Luhrmann R, Li J, Nagai K (1999) Crystal structures of two Sm protein complexes and their implications for the assembly of the spliceosomal snRNPs. *Cell* 96: 375–387

- Kamenska A, Simpson C, Vindry C, Broomhead H, Benard M, Ernoult-Lange M, Lee BP, Harries LW, Weil D, Standart N (2016) The DDX6-4E-T interaction mediates translational repression and P-body assembly. *Nucleic Acids Res* 44: 6318–6334
- Kean MJ, Couzens AL, Gingras AC (2012) Mass spectrometry approaches to study mammalian kinase and phosphatase associated proteins. *Methods* 57: 400–408
- Marnef A, Sommerville J, Ladomery MR (2009) RAP55: insights into an evolutionarily conserved protein family. *Int J Biochem Cell Biol* 41: 977–981
- Matsumoto K, Nakayama H, Yoshimura M, Masuda A, Dohmae N, Matsumoto S, Tsujimoto M (2012) PRMT1 is required for RAP55 to localize to processing bodies. *RNA Biol* 9: 610–623
- McCoy AJ, Grosse-Kunstleve RW, Adams PD, Winn MD, Storoni LC, Read RJ (2007) Phaser crystallographic software. *J Appl Crystallogr* 40: 658–674
- Nishimura T, Padamsi Z, Fakim H, Milette S, Dunham WH, Gingras AC, Fabian MR (2015) The eIF4E-binding protein 4E-T is a component of the mRNA decay machinery that bridges the 5' and 3' termini of target mRNAs. *Cell Rep* 11: 1425–1436
- Ozgur S, Basquin J, Kamenska A, Filipowicz W, Standart N, Conti E (2015) Structure of a human 4E-T/DDX6/CNOT1 complex reveals the different interplay of DDX6-binding proteins with the CCR4-NOT complex. *Cell Rep* 13: 703–711
- Poornima G, Shah S, Vignesh V, Parker R, Rajyaguru PI (2016) Arginine methylation promotes translation repression activity of eIF4G-binding protein, Scd6. *Nucleic Acids Res* 44: 9358–9368
- Rajyaguru P, She M, Parker R (2012) Scd6 targets eIF4G to repress translation: RGG motif proteins as a class of eIF4G-binding proteins. *Mol Cell* 45: 244–254
- Schutz S, Noldeke ER, Sprangers R (2017) A synergistic network of interactions promotes the formation of *in vitro* processing bodies and protects mRNA against decapping. *Nucleic Acids Res* 45: 6911–6922
- Sharif H, Ozgur S, Sharma K, Basquin C, Urlaub H, Conti E (2013) Structural analysis of the yeast Dhh1-Pat1 complex reveals how Dhh1 engages Pat1, Edc3 and RNA in mutually exclusive interactions. *Nucleic Acids Res* 41: 8377–8390
- Sweet T, Kovalak C, Collier J (2012) The DEAD-box protein Dhh1 promotes decapping by slowing ribosome movement. *PLoS Biol* 10: e1001342
- Tanaka KJ, Ogawa K, Takagi M, Imamoto N, Matsumoto K, Tsujimoto M (2006) RAP55, a cytoplasmic mRNP component, represses translation in *Xenopus* oocytes. *J Biol Chem* 281: 40096–40106
- Tritschler F, Eulalio A, Truffault V, Hartmann MD, Helms S, Schmidt S, Coles M, Izaurralde E, Weichenrieder O (2007) A divergent Sm fold in EDC3 proteins mediates DCP1 binding and P-body targeting. *Mol Cell Biol* 27: 8600–8611
- Tritschler F, Eulalio A, Helms S, Schmidt S, Coles M, Weichenrieder O, Izaurralde E, Truffault V (2008) Similar modes of interaction enable Trailer Hitch and EDC3 to associate with DCP1 and Me31B in distinct protein complexes. *Mol Cell Biol* 28: 6695–6708
- Tritschler F, Braun JE, Eulalio A, Truffault V, Izaurralde E, Weichenrieder O (2009) Structural basis for the mutually exclusive anchoring of P body components EDC3 and Tral to the DEAD box protein DDX6/Me31B. *Mol Cell* 33: 661–668
- Yang WH, Yu JH, Gulick T, Bloch KD, Bloch DB (2006) RNA-associated protein 55 (RAP55) localizes to mRNA processing bodies and stress granules. *RNA* 12: 547–554
- Zhang X, Zhang F, Guo L, Wang Y, Zhang P, Wang R, Zhang N, Chen R (2013) Interactome analysis reveals that C1QBP (complement component 1, q subcomponent binding protein) is associated with cancer cell chemotaxis and metastasis. *Mol Cell Proteomics* 12: 3199–3209
- Zipprich JT, Bhattacharyya S, Mathys H, Filipowicz W (2009) Importance of the C-terminal domain of the human GW182 protein TNRC6C for translational repression. *RNA* 15: 781–793